This article was downloaded by: [University of Tokyo]
On: 10 July 2012, At: 17:01
Publisher: Taylor & Francis
Informa Ltd Registered in England and Wales Registered Number: 1072954 Registered office: Mortimer House, 37-41 Mortimer Street, London W1T 3JH, UK

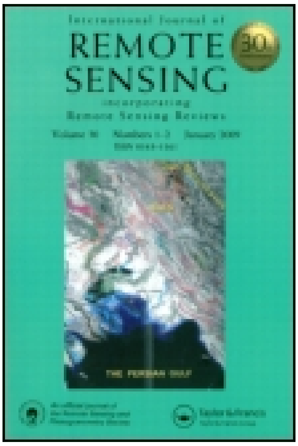

International Journal of Remote Sensing
Publication details, including instructions for authors and subscription information:
http://www.tandfonline.com/loi/tres20

Using multiscale texture information from ALOS PALSAR to map tropical forest

Preesan Rakwatin [a], Nicolas Longépé [b], Osamu Isoguchi [c], Masanobu Shimada [c], Yumiko Uryu [d] & Wataru Takeuchi [e]

[a] Geo-Informatics and Space Technology Development Agency (Public Organization), Lak Si, Bangkok, 10210, Thailand

[b] Collecte Localization Satellites (CLS), Plouzane, 29280, France

[c] Earth Observation Research Centre, Japan Aerospace Exploration Agency, Tsukuba Space Centre, Tsukuba, Ibaraki, 305-8505, Japan

[d] World Wildlife Fund (WWF), Washington, DC, 20037, USA

[e] Institute of Industrial Science, The University of Tokyo, Meguro, Tokyo, 153-8505, Japan

Version of record first published: 06 Jul 2012

To cite this article: Preesan Rakwatin, Nicolas Longépé, Osamu Isoguchi, Masanobu Shimada, Yumiko Uryu & Wataru Takeuchi (2012): Using multiscale texture information from ALOS PALSAR to map tropical forest, International Journal of Remote Sensing, 33:24, 7727-7746

To link to this article: http://dx.doi.org/10.1080/01431161.2012.701349

PLEASE SCROLL DOWN FOR ARTICLE

Full terms and conditions of use: http://www.tandfonline.com/page/terms-and-conditions

This article may be used for research, teaching, and private study purposes. Any substantial or systematic reproduction, redistribution, reselling, loan, sub-licensing, systematic supply, or distribution in any form to anyone is expressly forbidden.

The publisher does not give any warranty express or implied or make any representation that the contents will be complete or accurate or up to date. The accuracy of any instructions, formulae, and drug doses should be independently verified with primary sources. The publisher shall not be liable for any loss, actions, claims, proceedings, demand, or costs or damages whatsoever or howsoever caused arising directly or indirectly in connection with or arising out of the use of this material.

Downloaded by [University of Tokyo] at 17:01 10 July 2012

International Journal of Remote Sensing
Vol. 33, No. 24, 20 December 2012, 7727–7746

Using multiscale texture information from ALOS PALSAR to map tropical forest

PREESAN RAKWATIN*†, NICOLAS LONGÉPÉ‡, OSAMU ISOGUCHI§, MASANOBU SHIMADA§, YUMIKO URYU¶ and WATARU TAKEUCHI|

†Geo-Informatics and Space Technology Development Agency (Public Organization), Lak Si, Bangkok 10210, Thailand

‡Collecte Localization Satellites (CLS), Plouzane 29280, France

§Earth Observation Research Centre, Japan Aerospace Exploration Agency, Tsukuba Space Centre, Tsukuba, Ibaraki 305-8505, Japan

¶World Wildlife Fund (WWF), Washington, DC 20037, USA

|Institute of Industrial Science, The University of Tokyo, Meguro, Tokyo 153-8505, Japan

(*Received 22 May 2011; in final form 12 March 2012*)

Downloaded by [University of Tokyo] at 17:01 10 July 2012

This research investigated the ability of the Advanced Land Observing Satellite (ALOS) Phased Array type L-band Synthetic Aperture Radar (PALSAR) to map tropical forest in central Sumatra, Indonesia. The study used PALSAR 50 m resolution orthorectified HH and HV data. As land-cover discrimination is difficult with only two bands (HH and HV), we added textures as additional information for classification. We calculated both first- and second-order texture features and studied the effects of texture window size, quantization scale and displacement length on discrimination capability. We found that rescaling to a lower number of grey levels (8 or 16) improved discrimination capability and that equal probability quantization was more effective than uniform quantization. Increasing displacement tended to reduce the discrimination capability. Low spatial resolution increased the discrimination capability because low spatial resolution features reduce the effects of noise. A larger number of features also improved discrimination capability. However, the amount of improvement depended on the window size. We used the optimum combination of backscatter amplitude and textures as input data into a supervised multi-resolution maximum likelihood classification. We found that including texture information improved the overall classification accuracy by 10%. However, there was significant confusion between natural forest and acacia plantations, as well as between oil palm and clear cuts, presumably because the backscatter and texture of these class pairs are very similar.

1. Introduction

Tropical forests account for 18% of annual CO_2 emissions. CO_2 is released due to deforestation and degradation following fire, resource extraction and draining of peat lands (IPCC 2007). Failure to reduce tropical deforestation could result in an additional release of 80–130 Gt of carbon into the atmosphere by 2100, which is comparable to all the carbon released during the last decade through the combustion of

*Corresponding author. Email: preesan@gistda.or.th

International Journal of Remote Sensing
ISSN 0143-1161 print/ISSN 1366-5901 online © 2012 Taylor & Francis
http://www.tandfonline.com
http://dx.doi.org/10.1080/01431161.2012.701349

global fossil fuels (Gaveau *et al*. 2009). For this reason, the conservation of tropical forest is critical to mitigate climate change.

Accurate inventories and monitoring of forest areas are critical for estimating CO_2 emissions. Remote sensing is probably the most reliable measurement tool for accurate forest monitoring over large areas. Optical remote sensing, with its capabilities of large area coverage and frequent revisits, provides a viable means to map forest coverage areas at local and regional levels. However, forest mapping with such imagery is often challenging in tropical regions, because in some seasons, these regions have frequent cloud cover and heavy precipitation. It is often difficult and sometimes impossible to acquire cloud-free images.

To avoid cloud effects, researchers have been using Synthetic Aperture Radar (SAR) data. SAR provides a promising alternative because it can penetrate clouds, as well as smoke and haze from fires. The Advanced Land Observing Satellite (ALOS) carries an SAR sensor called Phased Array L-band Synthetic Aperture Radar (PALSAR). ALOS was launched on 24 January 2006. PALSAR is expected to play a key role in estimating the loss of the forest-cover and land-cover change. The L-band SAR sensor penetrates the above-ground biomass of tree trunks and canopies, independent of atmospheric conditions and observation time (day vs night) (Rosenqvist *et al*. 2007).

This study examines the potential of ALOS PALSAR 50 m spatial resolution data at HH and HV polarizations for mapping tropical rain forest in central Sumatra, Indonesia. In cooperation with the World Wildlife Fund (WWF), we selected Riau province, in central Sumatra, as a test site. Riau hosts some of the world's most biodiverse ecosystems. The province is covered by vast peatlands estimated to hold Indonesia's largest store of carbon. However, Riau has been under serious threat because of rapid large-scale deforestation (Uryu *et al*. 2008).

As the two bands of ALOS PALSAR were expected to provide limited ability to differentiate land cover, texture was used as an additional information source for classifying tropical rain forest (Nyoungui *et al*. 2002, Podest and Saatchi 2002). A large number of techniques for texture analysis have been investigated for SAR image classification. The two methods considered in this study are the first- and second-order texture statistics (Haralick 1979). This study focuses on comparing simple first- and second-order textures at multiple scales in order to evaluate their contributions to land-cover classification accuracy.

Although texture analysis in general has been widely investigated, there are some studies that have examined how various parameters may affect the ability of texture features to discriminate land cover (Van Der Sanden 1997, Podest and Saatchi 2002, Kayitakire *et al*. 2006, Pacifici *et al*. 2009, Sarker and Nichol 2011). Therefore, we investigated the effects of texture window size, quantization scales and displacement length on the ability to discriminate between selected regions of interest. In this research, various combinations of texture features were selected using transformed divergence (TD) (Swain and Davis 1978), which calculates the statistical distance between land-cover classes.

After we investigated the relative efficiency of different textural features and parameters, we used principal component analysis (PCA) to integrate the backscattering and texture features. PCA can reduce the dimensionality of the data while preserving discrimination capability. First, four components from the PCA were used as input into a maximum likelihood (ML) classifier (Alesheikh and Fard 2007). The results were compared with an ML classifier based on backscattering information alone.

Downloaded by [University of Tokyo] at 17:01 10 July 2012

2. Study area, data set and evaluation data set

2.1 *Study area*

Riau province, central Sumatra, Indonesia, was selected as our study area. This province is rich with natural resources, particularly petroleum, natural gas, oil palm and fibre plantations. The climate in Riau is equatorial tropical climate, with two main seasons – the rainy season from November to April and dry season from June to September. The average temperature is 30°C during the day and 23°C at night throughout the year. Rainfall is between 2000 and 3000 mm/year on average. The province was once heavily forested lowlands, but as oil palm plantations and logging have become major industries, it is now losing around 2000 km^2 of forest per year. In 2007, the forest cover had dropped to 27% (or 22 000 km^2) from 78% (or 64 000 km^2) in 1982.

Riau regularly suffers from smoke and haze due to land-clearing fires for oil palm plantations during dry seasons. The fires occur because businesses, community cooperation units and individual community members slash and burn the natural forest in order to replace it with oil palm plantation. At present, the deforestation in Riau is largely driven by industrial plantation companies. Heavy machinery is used to build roads into the forest and to clear cut the trees. According to Uryu *et al*. (2008), 29% of forest cover was cleared for industrial oil palm plantation, whereas 24% was cleared for industrial pulpwood plantations.

Downloaded by [University of Tokyo] at 17:01 10 July 2012

2.2 *PALSAR data sets*

Two 50 m orthorectified PALSAR data sets were selected within the Riau province as shown in figure 1. Figure 1(*a*) shows the 443rd strip image, taken on 28 June 2007. Figure 1(*b*) shows the 444th strip image, taken on 30 November 2007. Even though this research did not consider seasonal difference, it is worth mentioning that the backscattering varies from the maximum to the minimum value, corresponding to the wet and dry seasons, respectively (Minchella *et al*. 2009, Tanase *et al*. 2011). The seasonality of the data is related to the moisture content. The dual-polarized HH and HV channels were projected into geographical latitude and longitude coordinates. HH means that the electromagnetic waves are transmitted as horizontally polarized signals, and then received as horizontally polarized signals. HV means that the electromagnetic waves are transmitted as horizontally polarized signals, but then received as vertically polarized signals. The SAR mosaicking algorithm used in this research was introduced by Shimada and Otaki (2010) and Shimada (2010). This algorithm can produce large-scale radiometrically and geometrically calibrated SAR data sets. Slope correction was applied using the Shuttle Radar Topography Mission (SRTM) 90 m Digital Elevation Model.

Each site covers about 40 700 km^2. These two sites are known for their intensive land-use change and deforestation. The difference between the two images is in terrain type and scales of plantation. The topography of the 443rd strip area is flat plain. Agro-industrial companies have plantations over large homogeneous areas. The 444th strip image has rugged terrain where small-scale plantations predominate. In both images, the main land-cover classes are forest, oil palm, acacia, clear cut and water. The rest of the area contains primary vegetation that has undergone logging, secondary growth or different types of cultivated land. Both large- and small-scale plantations occur throughout the study areas.

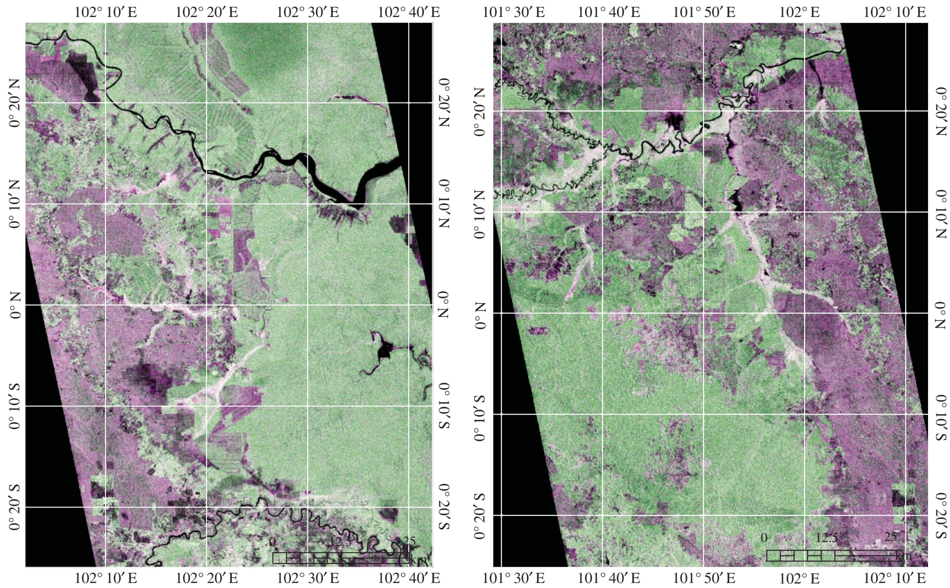

(*a*) (*b*)

Figure 1. PALSAR 50 m orthorectified mosaic product over the Riau province as colour composites of σ^0_{HH} (red), σ^0_{HV} (green) and σ^0_{HH} (blue). Channels have been stretched for the purpose of contrast enhancement. Images were acquired on (*a*) 28 June 2007 (strip 443) and (*b*) 30 November 2007 (strip 444).

For PALSAR standard products (level 1.5) provided by JAXA, the conversion between the amplitude (DN) and the normalized radar cross-section in decibel (σ^0) is given as follows (Shimada *et al*. 2009).

$$\sigma^0 = 10 \times \log_{10} \langle \mathrm{DN}^2 \rangle + \mathrm{CF}, \tag{1}$$

with the calibration factor (CF), which depends on the process date (in this case, CF is equal to -83 for both HH and HV).

2.3 *Evaluation data set*

For ground truth, this study used the 2007 WWF Riau GIS Land Cover Database. To create this database, WWF experts visually interpreted Landsat ETM images with the minimum mapping unit fixed at 50 ha. The land-cover areas were digitized at a scale of 1:90 000. The accuracy of the land-cover map was confirmed by frequent field verification (Uryu *et al*. 2008). Both test areas are covered by the same Landsat ETM image taken on 4 April 2007 (path/row = 126/060).

3. Methods

3.1 *Rescaled image creation and region of interest selection*

The first step in our analysis created backscatter and texture images at different spatial resolutions (400 and 200 m). Backscatter (HH/HV) and texture images were computed over window sizes with increasing dyadic scales of 8×8 window sizes and 4×4

Downloaded by [University of Tokyo] at 17:01 10 July 2012

Table 1. Summary of features.

PALSAR channels	Quantization Method	Quantization Scale	Window size	Distance range	Features
HH	Equal Prob.	8, 16, 32	8	1, 2, 3, 4, 5, 6	7 (First)
HV	Uniform	64, 128, 256	4	1, 2	6 (Second)

window sizes, respectively. Average backscattering at 400 and 200 m resolution scale is expressed by the mean radar cross-section per unit projected area. Each textural feature image was computed according to the texture feature definitions. For each SAR image, the normalized cross-section data were rescaled to obtain output images with 256, 128, 64, 32, 16 and 8 quantization levels using both uniform and equal probability quantizations. We calculated seven first-order texture features for both 400 and 200 m resolution scales. At 400 m resolution scale, a series of six second-order texture features corresponding to displacement lengths ranging from 1 to 6 pixels was computed. For 200 m resolution scale, we used displacement lengths of 1 and 2. Hence, the total number of images extracted per region was equal to 1322 features. A summary of all of the parameters derived in this study is presented in table 1.

Then, we identified the image regions representing the land-cover types studied. Regions of interest (ROIs) were identified over the whole images. Thirty ROIs were selected to analyse the discrimination capability of different textural parameters. For each spatial resolution, the same identified ROIs were used to extract backscattering values and textural features from the SAR data.

3.2 *Extraction of texture features*

Texture is defined as spatial variations in the image data. It carries useful information for discriminating between classes. Previous research haves shown that texture information can enhance classification accuracy using SAR data (Podest and Saatchi 2002). There are various methods for extracting textural information from different order histograms of an image using various degrees of statistics (Milne and Dong 2002). Many applications have adopted methods based on grey-level co-occurrence matrix (GLCM) or Markov random field models (Clausi and Yue 2004). Grandi *et al*. (2009) analysed spatial statistics in SAR data using wavelet frames for characterizing structural properties of forests. Podest and Saatchi (2002) used various combinations of texture measurements at different scales to aid the class discrimination. It is generally assumed that the radar backscattering and textures have normal distributions (Podest and Saatchi 2002) and can be used as inputs to a supervised ML classification.

In SAR images, however, grey level variations result not only from the spatial variability in the scattering properties of the object observed (texture) but also from the presence of speckle. Speckle in SAR images is usually modelled as multiplicative random noise. According to Hoekman (1991), speckle variance for logarithmically scaled radar intensity is independent of the texture variance. The speckle variance depends on the number of looks only. Logarithmically scaled radar intensity images are therefore more appropriate for use in textural analysis than either linearly scaled radar amplitude or intensity images. Therefore, this research used logarithmically scaled radar

Downloaded by [University of Tokyo] at 17:01 10 July 2012

intensity to measure class discrimination capability and to improve its classification accuracy.

In this research, several texture features derived from SAR data were investigated to determine their capability to discriminate classes. The texture features, based on first- and second-order statistics, are described in §§3.2.2 and 3.2.3.

3.2.1 Quantization schemes. Quantization is an important consideration in the computation of texture, especially GLCM. This is because the more the grey scale levels are used, the more the computation cost increases. The quantization method also has the potential to enhance texture information. This research compares two quantization schemes: (1) linear or uniform quantization and (2) equal probability quantization. For linear quantization, the bin size is fixed. A constant quantization bin size is used no matter what the instantaneous grey level distribution is. In the equal probability quantization scheme, each bin has a similar probability. Equal probability quantization has been shown to accurately represent the original image in terms of GLCM-based textures (Soh and Tsatsoulis 1999).

3.2.2 First-order texture statistics. For each pixel, the texture features are derived from first-order histograms over the surrounding window. A first-order histogram describes the frequency of occurrence of each grey level within the window. First-order histograms have been used extensively to quantify texture in SAR images (Saatchi *et al.* 2000, Nyoungui *et al.* 2002, Podest and Saatchi 2002, Kuplich and Curran 2005). Further descriptions of the textures can be found in Haralick and Shaunmugam (1973). The seven first-order texture measurements that we used are presented in table 2. For first-order texture, $p(i)$ is the frequency of grey level i occurring in a pixel window, whereas N_g represents the quantization level of the image g.

Table 2. Texture measures derived from local statistic, first-order and second-order textures.

Texture type	Feature	Formula
First-order	Mean	$\mathrm{AVG} = \mu = \sum_{i=1}^{N_g} ip(i)$
	Variance	$\mathrm{VAR} = \sigma^2 = \frac{1}{N_g}\sum_{i=1}^{N_g}(i-\mu)^2$
	Energy	$\mathrm{ENG} = -\sum_{i=1}^{N_g} p(i)^2$
	Entropy	$\mathrm{ENT} = -\sum_{i=1}^{N_g} p(i)\ln p(i)$
	Coefficient of variation	$\mathrm{CV} = \frac{\sigma}{\mu}$
	Skewness	$\mathrm{SKW} = \frac{1}{\sigma^3}\left[\sum_{i=1}^{N_g}(i=\mu)^3 p(i)\right]$
	Kurtosis	$\mathrm{KUR} = \frac{1}{\sigma^4}\left[\sum_{i=1}^{N_g}(i-\mu)^4 p(i) - 3\right]$
Second-order	Angular second moment	$\mathrm{ASM} = \sum_{i=1}^{N_g}\sum_{j=1}^{N_g} p^2(i,j)$
	Contrast	$\mathrm{CON} = \sum_{i=1}^{N_g}\sum_{j=1}^{N_g} p(i,j)(i-j)^2$
	Correlation	$\mathrm{COR} = \sum_{i=1}^{N_g}\sum_{j=1}^{N_g} p(i,j)\frac{(i-m_x)(j-m_y)}{s_x s_y}$
	Entropy	$\mathrm{ENT} = -\sum_{i=1}^{N_g}\sum_{j=1}^{N_g} p(i,j)\ln p(i,j)$
	Inverse difference moment	$\mathrm{IDM} = \Sigma_{i=1}^{N_g}\sum_{j=1}^{N_g}\frac{p(i,j)}{1+(i-j)^2}$
	Maximum probability	$\mathrm{MAX} = \max_{ij} p(i,j)$

Downloaded by [University of Tokyo] at 17:01 10 July 2012

3.2.3 Second-order texture statistics. Second-order texture measurements based on Haralick's GLCMs (Haralick and Shaunmugam 1973) consider the distance and angular spatial relationships between pixels within a window. The GLCM computes the joint probability of occurrence of pairs of grey levels separated by a given distance and direction. In this study, GLCM textures were calculated for all directions (omni directional) for representing variance measured within a window.

A number of statistical measurements that have been used effectively in many SAR applications (Soh and Tsatsoulis 1999, Kuplich and Curran 2005) can be extracted from the GLCM. This research used six second-order texture measurements, shown in table 2. For second-order texture, N_g is the quantization level of the image. $p(i, j)$ is the relative frequency of grey levels i and j which two neighbouring pixels separated by a distance of Δx columns and Δy lines (Kuplich and Curran 2005). For GLCM-based correlation, the mean (μ) and the standard deviation (s) are derived from

$$\begin{gathered}\mu_I = \sum\nolimits_i ip(i,*) \quad \mu_J = \sum\nolimits_j jp(*,j) \\ s_I = \sqrt{\sum\nolimits_i (i-\mu_I)^2 p(i,*)} \quad s_J = \sqrt{\sum\nolimits_j (j-\mu_J)^2 p(*,j)},\end{gathered} \tag{2}$$

where

$$p(i,*) = \sum_j p(i,j) \quad p(*,j) = \sum_i p(i,j). \tag{3}$$

3.3 *Evaluation of discrimination capability*

For each spatial scale, the potential texture features used in the classification were selected by TD. TD evaluates a feature's performance in class discrimination by calculating the statistical distance between each pair of classes included in the image. This is an indirect, *a priori* estimate of the probability of correct classification (Swain and Davis 1978). The TD for class pair (a, b) is given by

$$TD_{\mathrm{ab}} = 2000\left(1 - e^{\frac{-D_{\mathrm{ab}}}{8}}\right), \tag{4}$$

with

$$D_{\mathrm{ab}} = \frac{1}{2}\mathrm{tr}\left[(\Sigma_{\mathrm{a}}-\Sigma_{\mathrm{b}})\left(\Sigma_{\mathrm{a}}^{-1}-\Sigma_{\mathrm{b}}^{-1}\right)\right] + \frac{1}{2}\mathrm{tr}\left[\left(\Sigma_{\mathrm{a}}^{-1}+\Sigma_{\mathrm{b}}^{-1}\right)(M_{\mathrm{a}}-M_{\mathrm{b}})(M_{\mathrm{a}}-M_{\mathrm{b}})^{\mathrm{T}}\right], \tag{5}$$

where Σ_{a} and Σ_{b} are the covariance matrices, Σ_{a}^{-1} and Σ_{b}^{-1} are the inverse covariance matrices and M_{a} and M_{b} are the mean vectors for classes a and b, respectively. tr is the trace of the matrix in question (sum of the diagonal elements), whereas T refers to the transposed matrix. The TD measure is based on the assumption that the classes follow normal distributions. The highest value of TD is 2000, which indicates the largest separability that the probability distributions of the two classes do not overlap at all. The value 2000 is arbitrary and varies across different studies.

This research used the value 2000 in agreement with the TD formula from Van Der Sanden (1997).

Downloaded by [University of Tokyo] at 17:01 10 July 2012

In this study, we wanted to find the best texture features for both first- and second-order textures and the effects of texture window size, quantization scale and displacement length on discrimination capability. In addition, we wanted to see how TD improved as we added more features. For these reasons, we chose a TD value greater than or equal to 1900 as our threshold to calculate how many of the studied class pairs could be successfully discriminated (Van Der Sanden 1997). A value of 1900 corresponds to a lower bound for the likelihood of correct classification of close to 78%. A maximum of 22% of one of the two classes may thus be misclassified.

3.4 *Multiscale classification*

An ML classification was used to classify all of the images used in this study. Figure 2 shows the flow chart of the proposed algorithm that was carried out to enhance the classification accuracy and efficiency of the ML classification method. The ML classification has been modified to use prior information along with a multiscale approach.

This research uses the initial resolution scale 50 m backscattering images to calculate textures at 200 and 400 m spatial resolutions. Window sizes larger than 8×8 pixels were disregarded because they do not provide any new information for homogeneous land-cover types and suffer from mixed-pixel problems. On the other hand, the window sizes less than 4×4 pixels were not analysed because they are too small to describe texture information of the land-cover class.

Using the low spatial resolution features (400 m), the optimum band combination of backscattering amplitude and texture features was selected based on TD. PCA

Downloaded by [University of Tokyo] at 17:01 10 July 2012

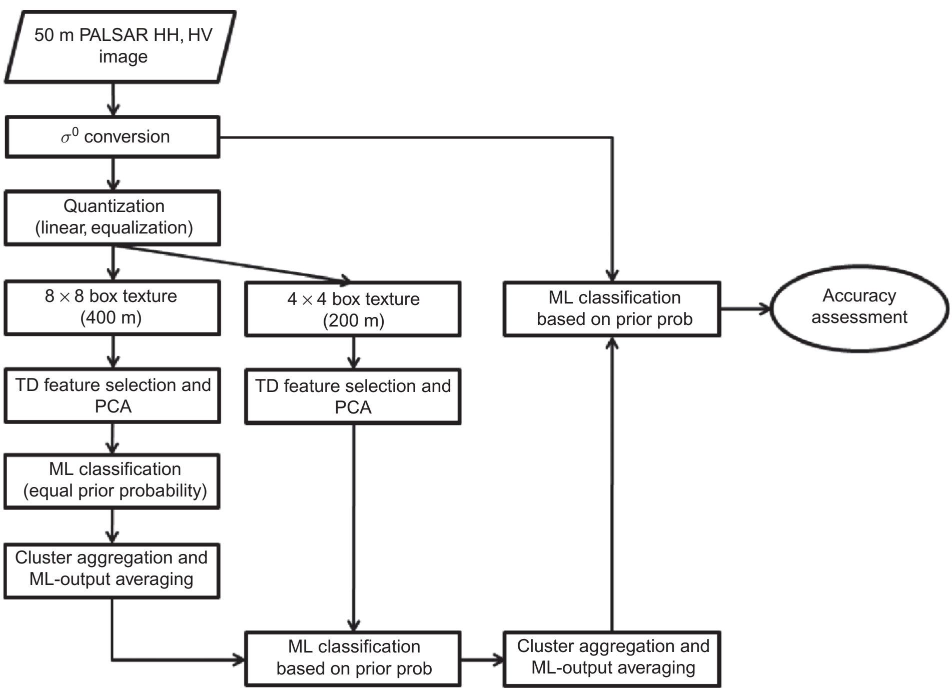

Figure 2. Flow chart of the classification process of SAR images.

was then employed to reduce dimensionality of the data, because the parameters are strongly interrelated. First, four components from the PCA were then processed by conventional ML classification. At this scale, the *a priori* probability is assumed to be equal for all of the classes. The results of the classifier at 400 m resolution scale are used as *a priori* probabilities for the 200 m resolution scale. The *a priori* probabilities are probabilities with which the class membership of a pixel could be guessed before classification (Podest and Saatchi 2002). A *priori* probabilities are represented by the first term, $p(\omega_i)$, in the discriminant function for ML classification.

$$g_i(\mathbf{x}) = \ln p(\omega_i) - \frac{1}{2}\ln|\Sigma_i| - \frac{1}{2}(\mathbf{x} - \mu_i)^{\mathrm{T}}\Sigma_i^{-1}(\mathbf{x} - \mu_i), \tag{6}$$

where x is the distance of the pixel pair in the horizontal axis and y is the distance of the pixel pair in the vertical axis.

The *a priori* probability when stepping from one scale to another is calculated for each pixel by

$$p(\omega_i) = \frac{g_i(\mathbf{x})}{\Sigma g(\mathbf{x})}. \tag{7}$$

The denominator is the sum over all classes of the discriminant function for the pixel. This research kept the probablity results for each class as separate layers to serve as input to the relaxation method decribed in §3.5.

3.5 *Relaxation method with spatial information*

The last step is the relaxation method that assigns a fixed class to each pixel. The simplest solution would assign the label, which is the most likely given the different posterior probabilities of equation (9) computed on a per-pixel basis. However, two neighbouring pixels are not totally independent and we would like to obtain continuous areas from the ML classifiers. In order to consider the spatial location of the pixels in the final decision, a clustering method based on a region-growing technique was implemented. Seed clusters were first computed based on a k-mean approach with the radiometric channel as input in order to enhance the processing speed. For each classifier, seed clusters were iteratively merged depending on their averaged $\langle p(\omega_i)\rangle$ values, with the L^1 norm metric being used to compute the distance with the centroids of neighbouring seed clusters. The smallest cluster was always considered first. A set of cluster-based averaged $\langle p(\omega_i)\rangle$ images was finally computed. As the clusters are computed for each class, the final labelling is finally performed on a per-pixel basis over the entire strip. This relaxation method takes into account both the posterior probabilities and the spatial information.

4. Results and discussion

4.1 *Separability evaluation of texture features*

Figures 3 and 4 illustrate the probability distribution of average backscattering of L band HH and HV at different resolution scales for data from the ROIs. Selected ROIs are forest (green), acacia (red), oil palm (magenta) and clear cut (orange). The probability density functions (pdf's) for L-band HH and HV are plotted at 400, 200, and 50 m resolution scales. Van Der Sanden (1997) showed that actual distributions of

Downloaded by [University of Tokyo] at 17:01 10 July 2012

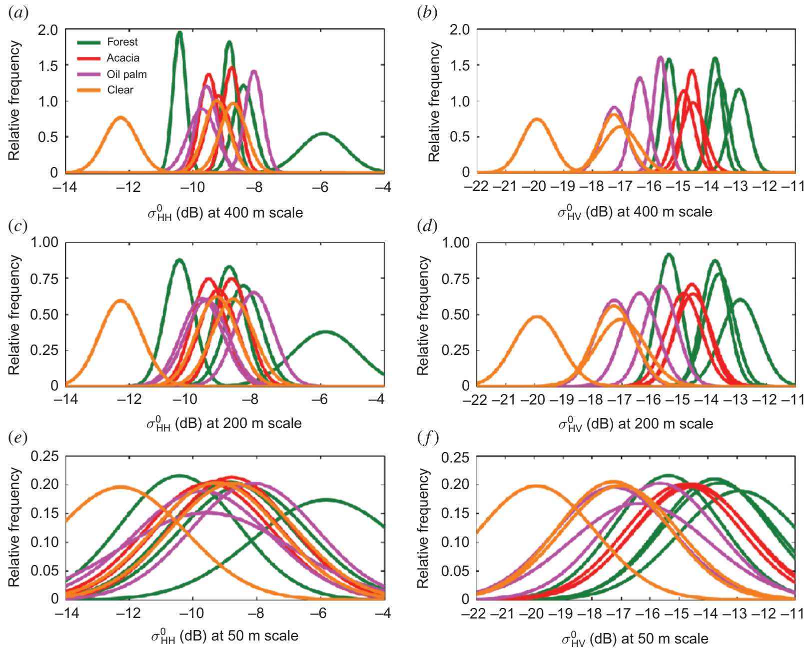

Figure 3. Gaussian probability distribution for region averaged backscatter associated with land-cover types present in the 443th strip image at 400 (*a*, *b*), 200 (*c*, *d*) and 50 m (*e*, *f*) scales. Peat forest is shown in dark green. Acacia is red, oil palm is magenta and clear cut is orange.

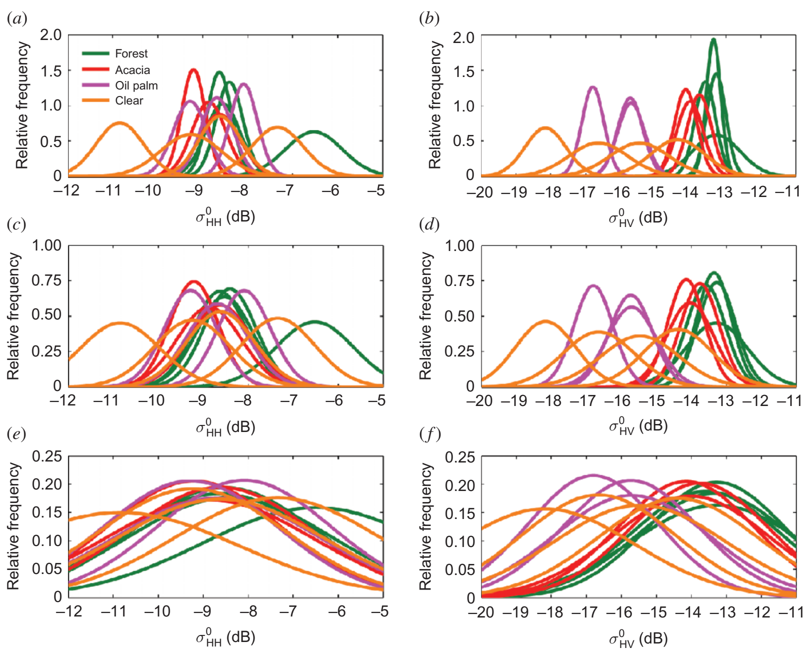

Figure 4. Gaussian probability distribution for region averaged backscatter associated with land-cover types present in the 444th strip image at 400 (*a*, *b*), 200 (*c*, *d*) and 50 m (*e*, *f*) m scales. Peat forest is shown in dark green. Acacia is red, oil palm is magenta and clear cut is orange.

Downloaded by [University of Tokyo] at 17:01 10 July 2012

selected land-cover type correspond to Gaussian approximations computed by linear averaging. This research uses the standard Matlab **normpdf** function to plot Gaussian distributions for specific mean and standard deviation values.

Figures 3 and 4 show that lower spatial resolutions can decrease the noise effects and increase separability of the land-cover classes. However, there is spectral variability within the same class. This variation is dependent on many factors such as the soil moisture, plant growth stage and terrain types. HV has better separability than HH as shown in Figures 3(*b*) and 4(*b*). HH seems to mix all of the classes. The HV band can clearly separate forest and oil palm/clear cut. The forest is uniform over the large area. However, there are some areas that have lower or higher backscatter than others. For HV, forest has an approximate backscattering value of –14 dB, whereas oil palm has its backscattering values at about –15 dB. Depending on the growth stage, acacia has very similar backscattering compared to forest for both HH and HV. If the acacia trees are still young, the backscattering is lower than the forest. Clear cut has high variation in backscattering values. It mostly has a lower backscatter value than forest and acacia. It is sometimes confused with oil palm.

Figures 5–8 show the analysis results of the texture discrimination capability with respect to texture window size, quantization scales and displacement length at 400 and 200 m spatial resolution. We found that energy and angular second moment have the highest discrimination capability for the first- and second-order statistical textures, respectively. In the figures, d01–d06 means angular second moment with displacements of 1–6 pixels. ENG means energy of the first-order texture. It can be seen that equal probability quantization leads to significant improvement compared with uniform quantization for both 400 and 200 m resolution scales. Depending on

Downloaded by [University of Tokyo] at 17:01 10 July 2012

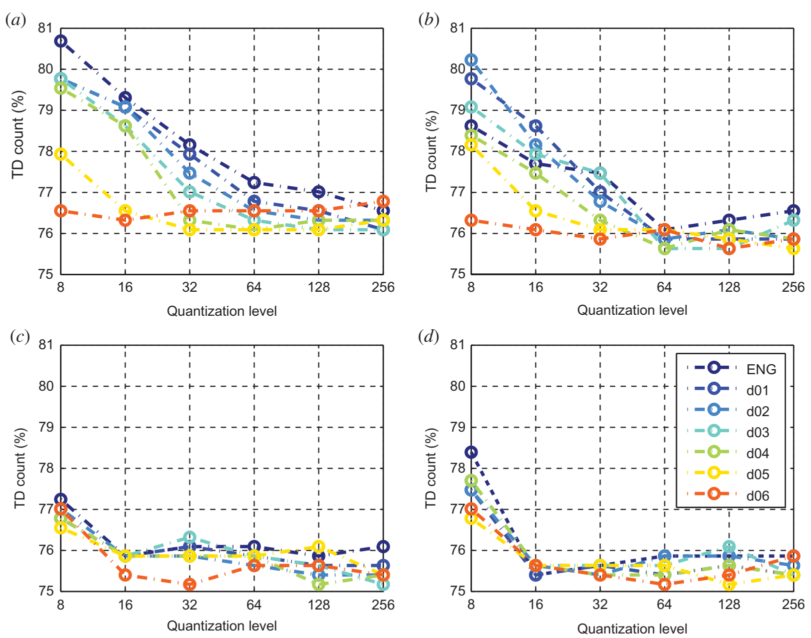

Figure 5. 443rd image plots relating TD count (%) and quantization level for 400 m resolution scale: (*a*) and (*b*) are HH and HV with equal probability quantization; (*c*) and (*d*) are HH and HV with uniform quantization. ENG is energy of first-order texture. d01–d06 mean displacement lengths of 1–6 pixels on angular second moment of second-order texture.

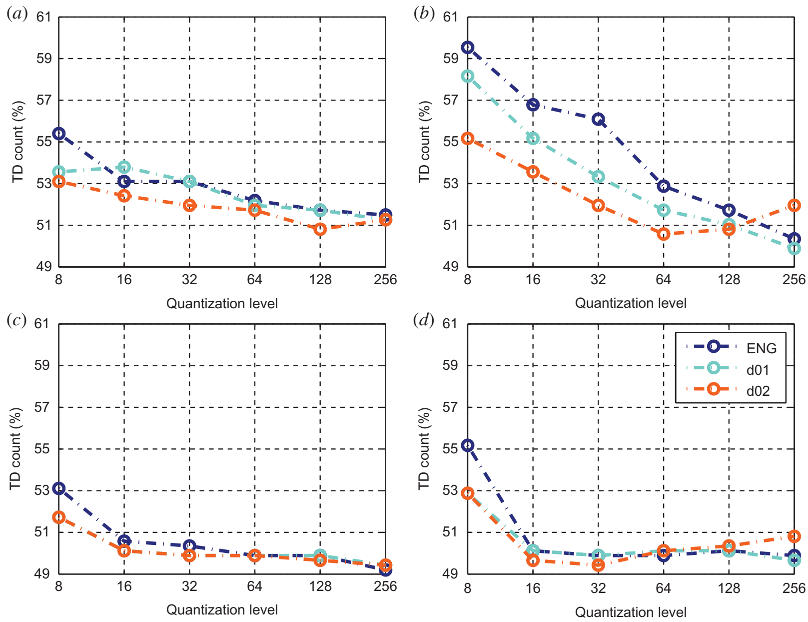

Figure 6. 443rd image plots relating TD count (%) and quantization level for 200 m resolution scale: (*a*) and (*b*) are HH and HV with equal probability quantization; (*c*) and (*d*) are HH and HV with uniform quantization. ENG is energy of first-order texture. d01–d02 mean displacement lengths of 1–2 pixels on angular second moment of second-order texture.

the quantization level, equal probability quantization offers around 80% TD count at 400 m scale whereas uniform quantization produces a TC count of about 76% for the 443rd strip. For the 200 m scale, equal probability quantization improves separability by about 5% compared with uniform quantization. A similar trend is observed for the 444th strip. However, overall discrimination appears somewhat poorer on this strip.

When considering the window size, the results show that lower spatial resolution increases the discriminating capacities of texture. This is due to the fact that lower spatial resolutions reduce variance in the texture measure due to the speckle noise. Figures 5 and 6 for the 443rd strip image show that the larger window size increases the number of pairs that can be discriminated by as much as 25% for HH and 21% for HV, for the 443rd strip image. Improvement of 37% for HH and 31% for HV can be seen for the 444th strip image.

The effects of number of grey levels (quantization) on the capacity of textures to identify the classes are shown in figures 5–8. For grey scale quantizing using equal probability quantization, the figures show that rescaling images to a lower number of grey levels does not weaken the ability of texture features to separate classes. Instead, a low number of grey levels produce high discrimination capability. For second-order statistic textures, a low number of grey levels considerably reduces the computational load, so textural analysis becomes more economical (Van Der Sanden 1997).

Comparison of figures 5 and 7 shows that the discrimination capability of the texture features computed with 256 grey scale levels is considerably poorer than that with 8 grey scale levels. The difference was approximately 4% for both HH and HV for the

Downloaded by [University of Tokyo] at 17:01 10 July 2012

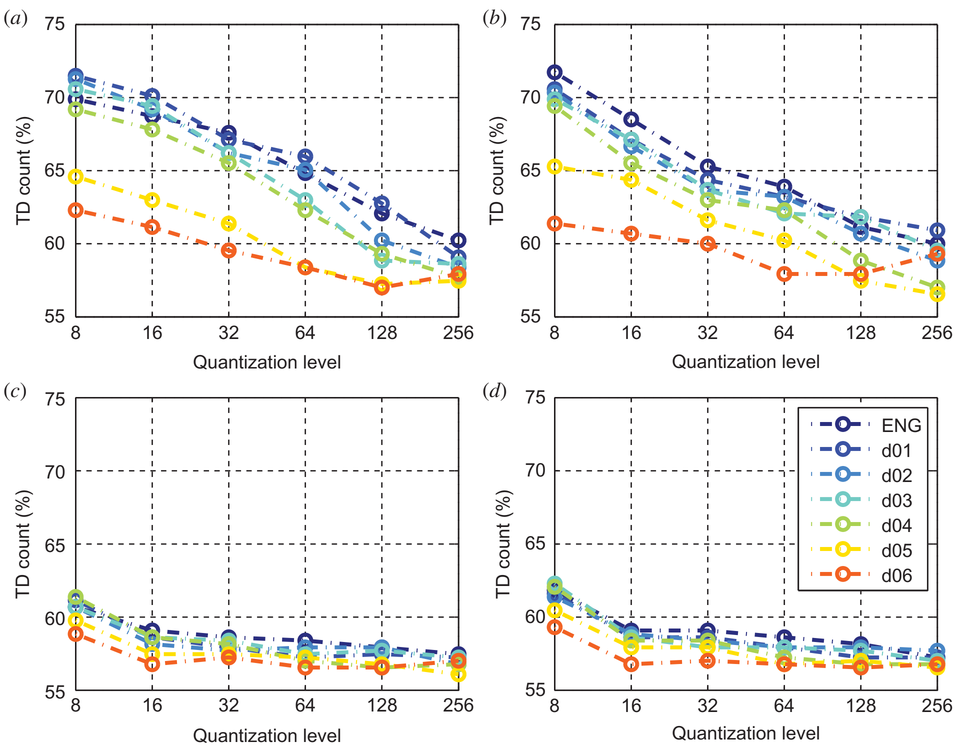

Figure 7. 444th image plots relating TD count (%) and quantization level for 400 m resolution scale: (*a*) and (*b*) are HH and HV with equal probability quantization; (*c*) and (*d*) are HH and HV with uniform quantization. ENG is energy of first-order texture. d01–d06 mean displacement lengths of 1–6 pixels on angular second moment of second-order texture.

Downloaded by [University of Tokyo] at 17:01 10 July 2012

443rd strip at 400 m scale resolution of the 443rd strip image. For 200 m scale resolution, the advantage of quantization was 2% for HH and 8% for HV. For 400 m scale resolution, the advantage of quantization was 10% for both HH and HV.

In the case of a statistic based on GLCM, the discrimination capability is best when the displacement is equal to one pixel and deteriorates when the displacement gets larger. Figure 5 shows that displacement with $d = 1$ produces an approximately 80% TD count compared with 76% with $d = 6$.

Figures 9 and 10 show the TD count (%) based on a number of features chosen as inputs to the ML classification at each resolution scale. Starting with the features that produced the highest TD count added features until it reached 100%. As expected, the TD count (%) tends to increase with an increase in the number of features. It is evident from figures 9 and 10 that the spatial resolution has a strong impact on the rate of increase in the TD count (%). Approximately 20 features at the 400 m resolution scale are needed to achieve perfect separability compared with 50 features at the 200 m resolution scale.

4.2 *Land-cover classification*

Section 4.1 has shown the ability of texture at different scales to discriminate between land-cover classes. Texture effectiveness appears to be related to the quantization level

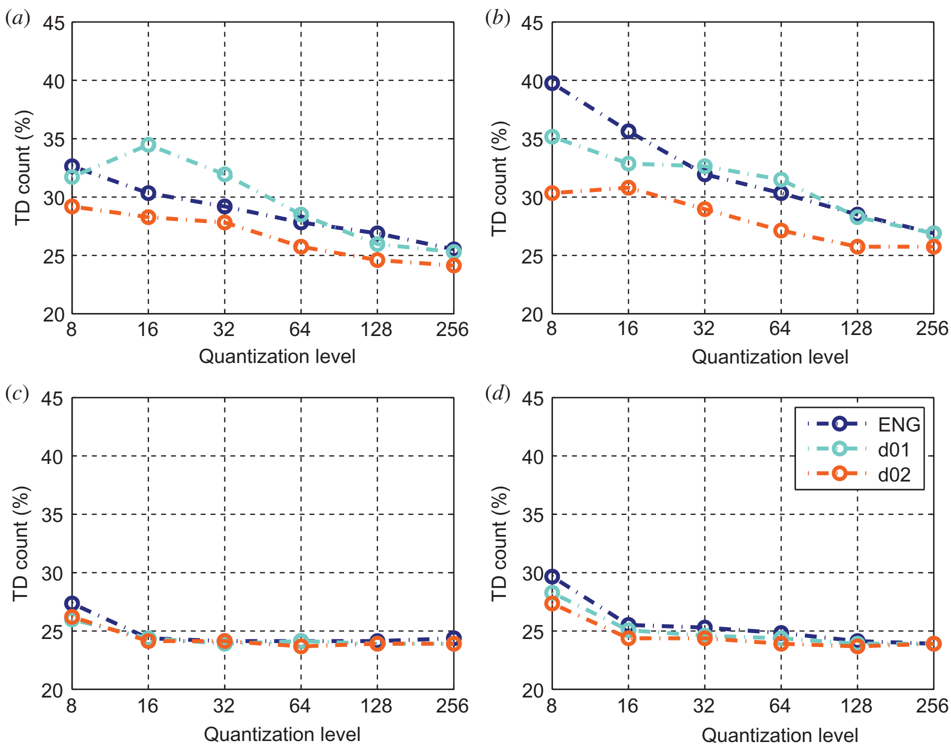

Figure 8. 444th image plots relating TD count (%) and quantization level for 200 m resolution scale: (*a*) and (*b*) are HH and HV with equal probability quantization; (*c*) and (*d*) are HH and HV with uniform quantization. ENG is energy of first-order texture. d01–d02 mean displacement lengths of 1–2 pixels on angular second moment of second-order texture.

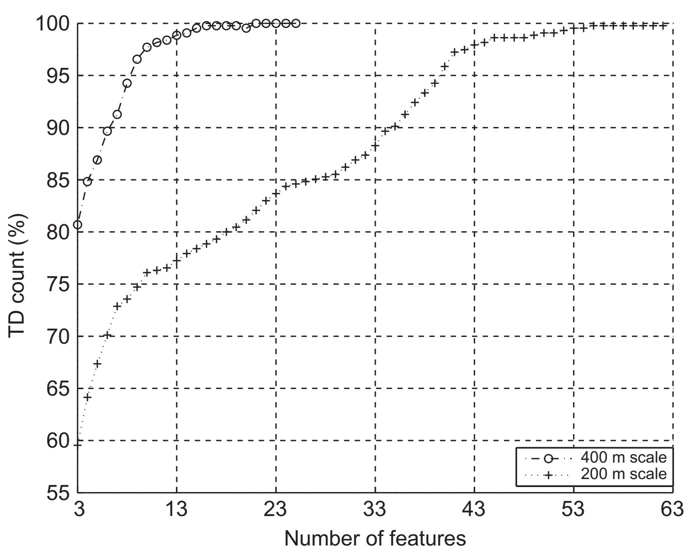

Figure 9. Variation of TD count (%) with the number of features for analysis based on training sets of 443th strip image at 400 and 200 m resolution scales.

Downloaded by [University of Tokyo] at 17:01 10 July 2012

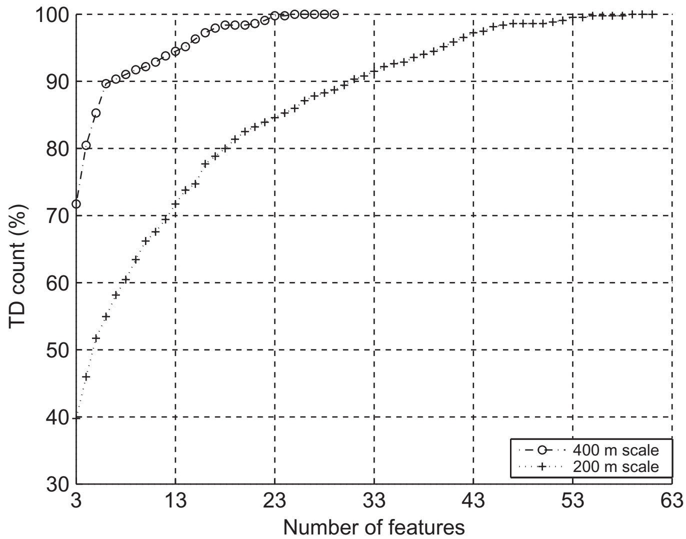

Figure 10. Variation of TD count (%) with the number of features for analysis based on training sets of 444th strip image at 400 and 200 m resolution scales.

Downloaded by [University of Tokyo] at 17:01 10 July 2012

and method, the displacement and the window size. This section discusses the classification results of ML classification with multiscale texture compared with that of ML classification alone.

Figures 11 and 12 show the classification results and 2007 WWF reference maps created using Landsat ETM data. We used five land-cover classes: forest, acacia, oil palm, clear cut and waterbody. Other regions that cannot be clearly identified by SAR images were grouped as a class named 'other' and were masked out of the calculation. Figures 11(*b*) and 12(*b*) show the classification results using multiscale ML classification. The visual appearance of the classification results shows a great improvement over the homogeneous areas compared to the classification results using 50 m pixel-to-pixel ML classification shown in figures 11(*a*) and 12(*a*). This is presumably because the multiscale ML classification also operates as a low-pass filter by eliminating the speckle and texture noise at 50 m scale.

For classification results using only backscatter information, the confusion matrices of 443rd and 444th strip images are shown in tables 3 and 4. The overall classification accuracies for these images are 59.86% and 53.41%, respectively. Tables 5 and 6 illustrate that the overall accuracies increased to approximately 73% and 64% for the 443rd and 444th strips, respectively, when texture features and multiscale classification are used.

Although some of the classes are clearly separated (such as forest and oil palm), there is significant confusion between natural forest and acacia plantation because the backscatter and the texture are very similar. This could be predicted based on the separability analysis shown in figures 3 and 4. Oil palm and clear cut are also frequently confused. In addition, acacia is a fast-growing tree. Therefore, time-lapse acquisition between WWF reference maps derived from Landsat and SAR data might introduce misclassification errors.

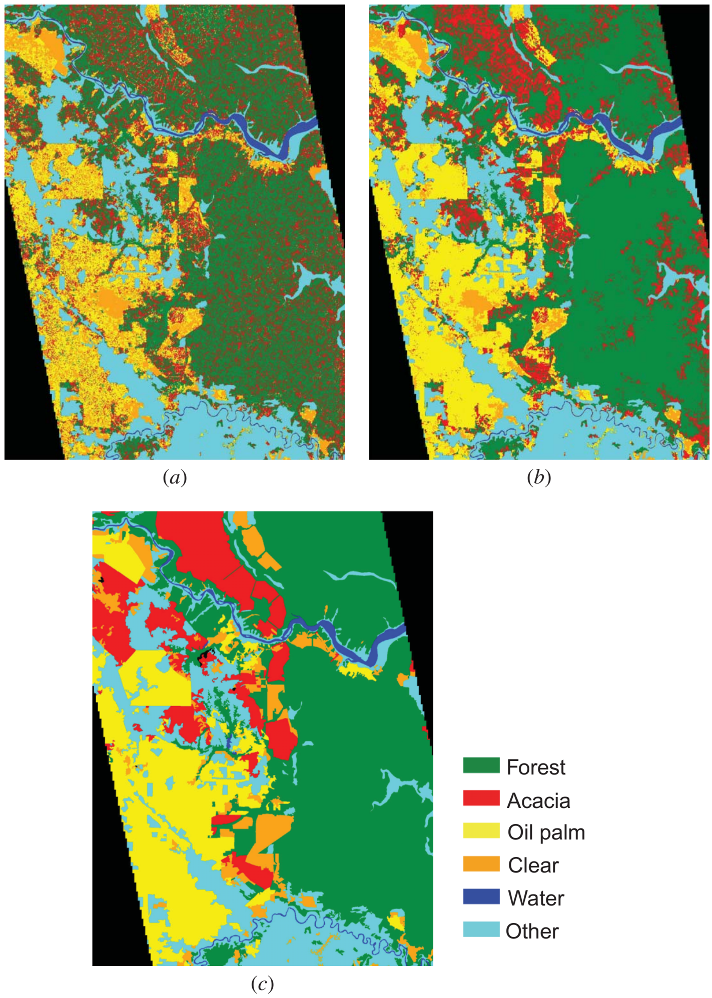

Figure 11. Classification results for the 443rd strip SAR image: (*a*) the 50 m pixel ML classification, (*b*) the 50 m multiscale classification and (*c*) the 2007 WWF ground data map. Peat forest is shown in dark green. Acacia is shown in red, oil palm is yellow, clear is orange, water is blue and other is cyan.

4.3 *Discussion*

To assess accuracy, we compared the PALSAR-based classification maps with the WWF reference map that was compiled from Landsat ETM. Note that the accuracy of classification maps in this study may be affected by temporal and spatial inconsistency between these data sources. The accuracy may also be reduced by the land-use change between the PALSAR acquisition periods and the Landsat ETM acquisition periods. The other hidden error may be due to the different spatial resolution of the data source. Landsat ETM has its spatial resolution at 30 m, whereas PALSAR mosaic products are generated at 50 m spatial resolution.

Downloaded by [University of Tokyo] at 17:01 10 July 2012

Downloaded by [University of Tokyo] at 17:01 10 July 2012

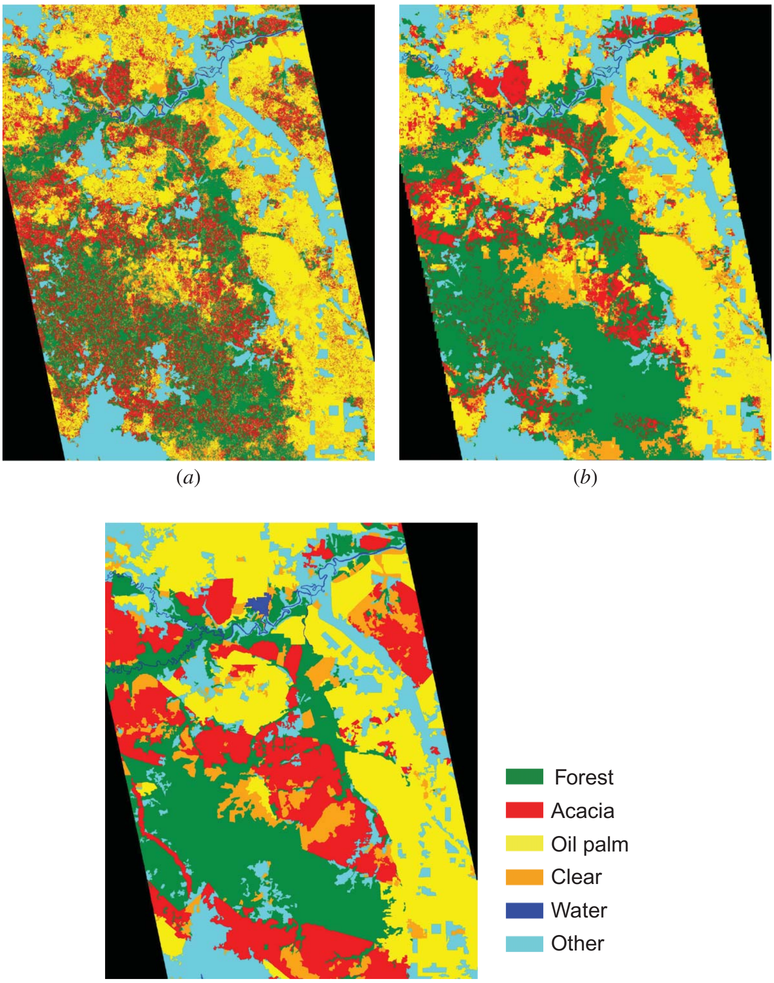

Figure 12. Classification results for the 444th strip SAR image: (*a*) the 50 m pixel ML classification, (*b*) the 50 m multiscale classification and (*c*) the 2007 WWF ground data map. Peat forest is shown in dark green. Acacia is shown in red, oil palm is yellow, clear is orange, water is blue and other is cyan.

Table 3. Confusion matrix for the 443th strip classified image by MLE based on L-band HH and HV backscatter (values in %).

	Forest	Oil palm	Acacia	Clear cut	Water	User's accuracy
Forest	72.1	8.99	50.79	15.01	3.14	79.60
Oil palm	1.92	51.4	9.7	33.68	9.47	68.45
Acacia	25.54	15.62	37.6	18.53	3.55	21.06
Clear cut	0.43	23.99	1.91	32.77	4.56	30.96
Water	0.01	0	0	0	79.27	99.54
					Overall accuracy = 59.86%	
					Kappa coefficient = 0.39	

Table 4. Confusion matrix for 444th strip classified image by MLE based on L-band HH and HV backscatter (values in %).

	Forest	Oil palm	Acacia	Clear cut	Water	User's accuracy
Forest	61.2	4.55	30.94	19.42	1.77	60.53
Oil palm	2.56	67.43	18.93	37.61	1.23	72.33
Acacia	22.12	9.94	35.01	17.73	1.7	43.88
Clear cut	14.11	18.08	15.12	25.24	7.51	14.16
Water	0.01	0	0	0	87.79	99.28
					Overall accuracy = 53.41%	
					Kappa coefficient = 0.36	

Table 5. Confusion matrix for 443th strip classified image by MLE based on L-band HH and HV backscatter and multiscale textures (values in %).

	Forest	Oil palm	Acacia	Clear cut	Water	User's accuracy
Forest	85.33	6.5	39.49	11.17	1.97	85.84
Oil palm	1.39	74.55	8.94	50.82	11.48	72.46
Acacia	13.11	8.04	50.94	17.01	4.2	39.75
Clear cut	0.17	10.9	0.62	20.99	2.59	39.08
Water	0.01	0	0	0	79.77	99.50
					Overall accuracy = 73.05%	
					Kappa coefficient = 0.57	

Table 6. Confusion matrix for 444th strip classified image by MLE based on L-band HH and HV backscatter and multiscale texture (values in %).

	Forest	Oil palm	Acacia	Clear cut	Water	User's accuracy
Forest	79.51	3.77	31.33	14.36	1.04	67.89
Oil palm	0.89	74.85	13.86	31.53	0.26	79.64
Acacia	9.15	5.16	40.84	16.83	0.75	63.54
Clear cut	10.42	16.20	13.97	37.25	11.09	22.04
Water	0.03	0.01	0	0.03	86.87	97.01
					Overall accuracy = 63.93%	
					Kappa coefficient = 0.50	

The overall classification accuracies for the 443rd strip image are better than for the 444th strip image. This is probably because the topography of the 444th strip area is hilly terrain. The land covers in this area are more spatially complex than in the 443rd strip image. Most of the deforested areas are owned by local villagers. In contrast with 444th strip, the 443rd strip area is located in flat terrain. The plantations in this area are operated by industrial companies and cover larger areas. For this reason, the land uses are more homogeneous than the 444th strip and thus produce higher classification accuracy. We also would like to mention that the backscattering varies from the maximum to the minimum value, corresponding to the wet and dry seasons, respectively. This is because the moisture content is related to the seasonal change.

Downloaded by [University of Tokyo] at 17:01 10 July 2012

5. Conclusion

In this research, we studied the potential for using ALOS PALSAR 50 m orthorectified L-band HH and HV data to map tropical forest. Detailed texture analysis was introduced as an additional information source. Our results showed that images rescaled to a lower number of grey levels (8 or 16) gave more accurate results as well as reducing computation time. Equal probability quantization schemes improved the separability between classes compared with uniform quantization. The displacement parameter also has an effect. There was a tendency for the discrimination capability to decrease when the displacement increased.

The analysis results demonstrated that lower spatial resolution improves the discrimination capability due to the fact that low spatial resolution reduces the effects of noise. Unsurprisingly, the number of feature used increases the discrimination capability. However, the rate depends on the window size (resolution).

This research used modified ML classification to identify land use. The classification strategy used a priori probabilities derived from the results of an ML classification at a more aggregated scale. The overall accuracies for land-cover classification increased by approximately 10% when combined with texture. However, we had difficulty in separating natural forest from acacia plantation and oil palm from clear cut. This is due to the fact that backscatter and texture of these class pairs are very similar.

Acknowledgements
This work was supported by the ALOS Kyoto and Carbon (K&C) Initiative project led by Earth Observation Research Centre (EORC), Japan Aerospace Exploration Agency (JAXA). The WWF Riau GIS Land Cover Database in 2007 was produced by Budi Setiabudi (SEAMEO Biotrop), Kokok Yulianto and Arif Budiman (WWF Indonesia).

Downloaded by [University of Tokyo] at 17:01 10 July 2012

References

Alesheikh, A. and Fard, F., 2007, Design and implementation of a knowledge-based system to improve maximum likelihood classification accuracy. *Canadian Journal of Remote Sensing*, **33**, pp. 459–467.

Clausi, D.A. and Yue, B., 2004, Comparing co-occurrence probabilities and Markov random fields for texture analysis of SAR sea ice imagery. *IEEE Transactions on Geoscience and Remote Sensing*, **42**, pp. 215–228.

Gaveau, D.L.A., Epting, J., Lyne, O., Linkie, M., Kumara, I., Kanninen, M. and Leader-Williams, N., 2009, Evaluating whether protected areas reduce tropical deforestation in Sumatra. *Journal of Biogeography*, **36**, pp. 2165–2175.

Grandi, G.D., Lucas, R. and Kropacek, J., 2009, Analysis by wavelet frames of spatial statistics in SAR data for characterizing structural properties of forests. *IEEE Transactions on Geoscience and Remote Sensing*, **47**, pp. 494–507.

Haralick, R., 1979, Statistical and structural approaches to texture. *Proceedings of the IEEE*, **76**, pp. 786–804.

Haralick, R. and Shaunmugam, K., 1973, Textural features for image classification. *IEEE Transactions on Systems, Man, and Cybernetics*, **3**, pp. 610–621.

Hoekman, D.H., 1991, Speckle ensemble statistics of logarithmically scaled data. *IEEE Transactions on Geoscience and Remote Sensing*, **29**, pp. 180–182.

IPCC, 2007, *Climate Change 2007: The Physical Science Basis: Summary for Policymakers* (Geneva: Intergovermental Panel on Climate Change).

Kayitakire, F., Hamel, C. and Defourny, P., 2006, Retrieving forest structure variables based on image texture analysis and IKONOS-2 imagery. *Remote Sensing of Environment*, **102**, pp. 390–401.

Kuplich, T. and Curran, P., 2005, Relating SAR image texture to the biomass of regenerating tropical forest. *International Journal of Remote Sensing*, **26**, pp. 4829–4854.

Milne, A. and Dong, Y., 2002, Vegetation mapping using JERS-1 SAR mosaic for northern Australia. *International Journal of Remote Sensing*, **23**, pp. 1475–1486.

Minchella, A., Frate, F.D., Capogna, F., Anselmi, S. and Manes, F., 2009, Use of multitemporal SAR data for monitoring vegetation recovery of Mediterranean burned areas. *Remote Sensing of Environment*, **113**, pp. 588–597.

Nyoungui, A., Tonye, E. and Akono, A., 2002, Evaluation of speckle filtering and texture analysis methods for land cover classification from SAR images. *International Journal of Remote Sensing*, **23**, pp. 1895–1925.

Pacifici, F., Chini, M. and Emery, W.J., 2009, A neural network approach using multi-scale textural metrics from very high-resolution panchromatic imagery for urban land-use classification. *Remote Sensing of Environment*, **113**, pp. 1276–1292.

Podest, E. and Saatchi, S., 2002, Application of multiscale texture in classifying JERS-1 radar data over tropical vegetation. *International Journal of Remote Sensing*, **23**, pp. 1487–1506.

Rosenqvist, A., Shimada, M., Ito, N. and Watanabe, M., 2007, ALOS PALSAR: a pathfinder mission for global-scale monitoring of the environment. *IEEE Transactions on Geoscience and Remote Sensing*, **45**, pp. 3307–3316.

Saatchi, S., Nelson, B., Podest, E. and Holt, J., 2000, Mapping land cover types in Amazon basin using 1 km JERS-1 mosaic. *International Journal of Remote Sensing*, **21**, pp. 1201–1234.

Sarker, L.R. and Nichol, J.E., 2011, Improved forest biomass estimates using ALOS AVNIR-2 texture indices. *Remote Sensing of Environment*, **115**, pp. 968–977.

Shimada, M., 2010, Ortho-rectification and slope correction of SAR data using DEM based simulated data and its accuracy evaluation. *IEEE Journal of Selected Topics in Applied Earth Observations and Remote Sensing*, **3**, pp. 657–671.

Shimada, M., Isoguchi, O., Tadono, T. and Isono, K., 2009, PALSAR radiometric calibration and geometric calibration. *IEEE Transactions on Geoscience and Remote Sensing*, **47**, pp. 3915–3932.

Shimada, M. and Otaki, T., 2010, Generating continent-scale high-quality SAR mosaic datasets: application to PALSAR data for global monitoring. *IEEE Journal of Selected Topics in Applied Earth Observations and Remote Sensing*, **3**, pp. 637–656.

Soh, L.K. and Tsatsoulis, C., 1999, Texture analysis of SAR sea ice imagery using gray level co-occurrence matrics. *IEEE Transactions on Geoscience and Remote Sensing*, **37**, pp. 780–795.

Swain, P.H. and Davis, S.M. (Eds.), 1978, *Remote Sensing; The Quantitative Approach* (New York: Mcgraw-Hill).

Tanase, M., de la Riva, J., Santoro, M., P´erez-Cabello, F. and Kasischke, E., 2011, Sensitivity of SAR data to post-fire forest regrowth in Mediterranean and boreal forests. *Remote Sensing of Environment*, **115**, pp. 2075–2085.

Uryu, U., Mott, C., Foead, N., Yulianto, K., Budiman, A., Setiabudi, Takkai, F., Nurasamus, Sunarto, Purastuti, E., Fadhli, E., Hutajulu, C., Jaenicke, J., Hatano, R., Siegert, F. and Stuwe, M., 2008, *Deforestation, Forest Degradation, Biodiversity Loss and* CO_2 *Emission in Riau, Sumatra, Indonesia*. Technical Report, WWF Indonesia, Jakarta, Indonesia.

Van Der Sanden, J., 1997, Radar remote sensing to support tropical forest management. PhD thesis, Department of Water Resources, Wageningen Agricultural University, Wageningen.

Downloaded by [University of Tokyo] at 17:01 10 July 2012